Chemical Product and Process Modeling

Volume 6, *Issue* 1 2011 *Article* 22

CFD Modelling of Global Mixing Parameters in a Peirce-Smith Converter with Comparison to Physical Modelling

Deside K. Chibwe, *University of Stellenbosch*
Guven Akdogan, *University of Stellenbosch*
Chris Aldrich, *University of Stellenbosch*
Rauf H. Eric, *University of Witwatersrand*

Recommended Citation:
Chibwe, Deside K.; Akdogan, Guven; Aldrich, Chris; and Eric, Rauf H. (2011) "CFD Modelling of Global Mixing Parameters in a Peirce-Smith Converter with Comparison to Physical Modelling," *Chemical Product and Process Modeling*: Vol. 6: Iss. 1, Article 22.
DOI: 10.2202/1934-2659.1584

CFD Modelling of Global Mixing Parameters in a Peirce-Smith Converter with Comparison to Physical Modelling

Deside K. Chibwe, Guven Akdogan, Chris Aldrich, and Rauf H. Eric

Abstract

The flow pattern and mixing in an industrial Peirce-Smith converter (PSC) has been experimentally and numerically studied using cold model simulations. The effects of air volumetric flow rate and presence of overlaying slag phase on matte on the flow structure and mixing were investigated. The 2-D and 3-D simulations of the three phase system were carried out using volume of fluid (VOF) and realizable k - ε turbulence model to account for the multiphase and turbulence nature of the flow respectively. These models were implemented using commercial Computational Fluid Dynamics (CFD) numerical code FLUENT. The cold model for physical simulations was a 1:5 horizontal cylindrical container made of Perspex with seven tuyeres on one side of the cylinder typifying a Peirce-Smith converter. Compressed air was blown into the cylinder through the tuyeres, simulating air or oxygen enriched air injection into the PSC. The matte and slag phases were simulated with water and kerosene respectively in this study. The influence of varying blowing conditions and simulated slag quantities on the bulk mixing was studied with five different air volumetric flow rates and five levels of simulated slag thickness. Mixing time results were evaluated in terms of total specific mixing power and two mixing time correlations were proposed for estimating mixing times in the model of PSC for low slag and high slag volumes. Both numerical and experimental simulations were in good agreement to predict the variation characteristics of the system in relation to global flow field variables set up in the converter through mathematical calculation of relevant integrated quantities of turbulence, Volume Fraction (VF) and velocity magnitudes. The findings revealed that both air volumetric flow rate and presence of the overlaying slag layer have profound effects on the mixing efficiency of the converter.

KEYWORDS: physical and numerical modelling, CFD, Peirce-Smith converter

Author Notes: The financial support received from NRF is greatly acknowledged. The authors also extends acknowledgement to the technical staff in the Process Engineering Laboratory for assistance with assembling model superstructure.

1. INTRODUCTION

Mixing has become important in submerged pyrometallurgical gas injection systems and has attracted much attention. Most of research on mixing and injection phenomena in gas/ liquid multiphase systems have been conducted for the steel making and ladle metallurgy ((Castillejos & Brimacombe (1987), Kim & Fruehan (1987), Mazumdar & Guthrie (1986), Sahai & Guthrie (1982), Sinha & McNallan (1985), Stapurewicz & Themelis (1987)). According to work done by Turkoglu & Farouk (1991), mixing intensity and efficiency has been defined by mixing time, T_{mix} which is the total time interval required to achieve a value within ±5% of the tracer concentration at every nodal location in the system after the introduction of tracer for a well-mixed bath.

Peirce – Smith converters are such a submerged injection process and have been used in the copper making and PGM smelting industries for more than a century for the purpose of removing iron and sulphur to obtain blister copper and converter matte respectively through exothermic chemical reactions. This process step is referred to as conversion (Liow & Gray (1990), Real et al. 2007). The conversion process used in removing iron and sulphur content in matte is a complex phenomenon involving phase interactions, many chemical reactions, associated heat generation as well as product formation (Kyllo & Richards 1998a).

The converter used is cylindrical horizontal reactor (circular canal geometry) where air at subsonic velocity (Mach < 1) is injected into matte through submerged tuyeres which come along the axis of the converter (Gonzalez et al. 2008). The converting process is semi continuous and auto-thermal. Since there are chemical reactions taking place with products being formed; quality and quantity of mixing is important. Mixing will promote chemical reactions, removing the products from reaction sites; minimize temperature and composition inhomogeneties caused by cold solid additions in the form of scrap, process ladle skulls, reverts and fluxes which is inherent to the converting processes (Mazumdar & Guthrie (1986), Sinha & McNallan (1985)).

Despite substantial amount of PSC operational existence, there has been an insufficiency of research on process engineering aspects of the process. Mixing and mass transfer in the converter are such key process parameters that have been little studied. Due to similarity of the basic concept in ladle injection and PSC, the core tenets of the works have been adopted in the past decades on process characterization research of PSC in an effort to address the challenges in productivity (Gray et al. 1984, Hoefele & Brimacombe (1979), Vaarno et al. 1998).

Macroscopic physical and numerical models of PSC have been developed to study multiphase fluid flow phenomena (Liow & Gray (1990), Vaarno et al.

1998, Koohi et al. 2008, Ramirez-Argaez 2008, Rosales et al. 2009, Valencia et al. 2004, Valencia et al. 2006)). These models have been used extensively in pyro-metallurgical operations to establish functional relationships of process variables such as reaction kinetics (Kyllo & Richards 1998b), injection dynamics (Schwarz 1996, Rosales et al. 1999, Valencia et al. 2002) and fluid flow behaviour (Han et al. 2001, Real et al. 2007, Valencia et al. 2004).

However, despite the bulk of numerical and experimental work on the subject of fundamental phenomenon of multiphase flow, little effort has been addressed to the understanding of the combined effect of blowing rates and presence of slag phase to the overall mixing performance of the converter which gives a rough estimation of bulk homogeneity attainment period after additions to molten matte. If proper mixing is not achieved in the reactors, fundamental consequences are chemical, thermal and particulate inhomogeneties resulting in undesirable variability in the final product composition.

In general, mixing can be quantitatively evaluated using a variety of techniques employing physical and numerical simulations. Turkoglu & Farouk (1991) investigated the effects of bath aspect ratio and gas injection rate on mixing characteristics by numerical simulations of a model of a bottom stirred ladle. The mixing efficiency was quantified by mixing time through numerical solution of a tracer concentration equation and the liquid circulation rate. In a later publication, Zhu et al. (1996) investigated the effects of gas flow rate, positions of nozzle, tracer and inclined wall on the flow pattern and mixing in a model of ladle. Using numerical simulation and quantifying flow field variables, they found that all variables considered had an influence on the mixing efficiency.

In a physical simulation case study of a Creosot-Loire Uddeholm (CLU) model to investigate the influence of gas flow rate and bath height on mixing time and solid-liquid mass-transfer rates, Nyoka et al. (2003) used a tracer dispersion technique to find the mixing time. In recent studies to explore the bottom injection as an alternative technique to improve the mixing efficiency in PSC, the mixing efficiency was measured by calculating the integral turbulent kinetic energy of the copper matte (Real et al. 2007, Gonzalez et al. 2008).

In this work, the dependence of mixing on volumetric air flow rate and simulated slag quantities for different matte and slag levels is investigated using a combination of physical and numerical modelling. A 1:5 water bath physical model of equivalent properties as the generic industrial PSC to carry out the experiments was designed using similarity principles. Isothermal transient multiphase 2-D and 3-D CFD numerical simulations were carried out. The CFD numerical code FLUENT software was used to solve the transient Navier-Stokes equations. The realizable $k-\varepsilon$ turbulent model and infinitesimal fluid element also known as volume of fluid (VOF) was used to model the turbulence nature and multiphase flow respectively.

DOI: 10.2202/1934-2659.1584

Geometric, dynamic and kinematic similarities were used in the design for equivalency between prototype (real industrial Peirce-Smith converter) and model since hydrodynamic studies on fluid flow are not concerned with thermal and chemical similarity effects (Mazumdar 1990). This work presents a hybrid analysis study on the influence of flow rate and slag phase simultaneously on the mixing efficiency in the PSC using physical and numerical modelling.

2. EXPERIMENTAL TECHNIQUE

Cold model studies were carried out in a horizontal Perspex cylinder, which is a slice of 1:5 scale model of the generic commercial Peirce – Smith converter given in **Figure 1**.

Figure 1: Physical 1:5 scale water bath model of the Peirce Smith converter

It has 1000mm internal length and 690mm internal diameter with seven tuyeres (air inlet tubes through which compressed air is purged into the model) on one side of the vessel, each with an internal inlet diameter of 8mm. The model was fitted to a steel cradle to minimize vibration effects on the model superstructure as well as experimental results. For simulation purposes, water, kerosene and air were used to represent matte, slag and air and/ or oxygen enriched air respectively. A PVC 2.5 inch cylindrical manifold served as a reservoir for compressed air at a constant line pressure supply of 5.5 bars.

An inline VPFlowMate (VPF-R120-M100-D1-S110-E200) digital mass flow meter which uses Thermal Mass Flow (TMF) principle was used to measure compressed air volumetric flow rate into the model. The flow meter was powered

with a Low Voltage Limited Current (LVLC) power source (+12...24VDC, 1A). A manometer arrangement was used to measure pressure differentials in orifice plates inserted into tuyere inlets, with pressure differentials being adjusted accordingly to ensure equal flow of air in all seven tuyeres. Boundary conditions for the numerical simulations were derived from the geometry, kinematic and dynamic parameters which form the basis of the physical experimental set-up. The results obtained from numerical simulations were compared with the physical model experiments.

2.1 Physical simulation and model description

Similarity using dimensionless numbers is the key feature in the development of physical models. In the design process, geometry, kinematic and dynamic similarities were observed through consideration of dimensionless numbers. Geometric similarity was observed using scale factor, λ on all physical dimensions and dynamic similarity achieved through Modified Froude number, N_{Fr}^{*} which accounts for density difference of melts and injection gas as well as velocity of purged gas. Scale factor and Modified Froude number are given in **Eqs. (1)** and **(2)** respectively.

$$\lambda = \frac{l_{\mathrm{mod}el}}{l_{ptype}} \tag{1}$$

Where λ, $l_{\mathrm{mod}el}$ (mm), l_{ptype} (mm) are scale factor, model physical dimension and prototype (real) converter physical dimension.

$$N_{Fr}^{*} = \frac{v_t^2 \rho_g}{g\left(\rho_l - \rho_g\right) d_o} \tag{2}$$

Here, N_{Fr}^{*} is Modified Froude number; v_t is tuyere air velocity (ms^{-1}); ρ_g is air density (kgm^{-3}), ρ_l is density of simulated matte (kgm^{-3}); g is acceleration due to gravity (ms^{-2}); d_o is tuyere diameter (m).

Kinematic similarity was observed between prototype and model through Morton number, N_{Mo} which incorporates surface tensions, viscosities and densities of the fluids, which is given by:

$$N_{Mo} = \frac{g\mu^4}{\rho_l \sigma^3} \tag{3}$$

DOI: 10.2202/1934-2659.1584

Where N_{Mo} is Morton number, μ is dynamic viscosity of liquid (Pas) and σ is surface tension of liquid (Nm^{-1}).The observation of similarities yielded dimensions, blowing conditions and physical properties of the fluids as summarised in **Table I**.

Table 1: Physical properties of the fluids, dimensions and blowing conditions of a generic industrial PSC and the model.

System		**Prototype**	**Model**
Geometry similarity	Converter length, m	9.14	1
	Converter inner diameter, m	3.46	0.690
	Number of tuyeres	42	7
Dynamic Similarity	Volumetric flow rate, Nm^3s^{-1}	7.55	0.0113
	Tuyere gas velocity, ms^{-1}	138.5	30
	Mach number	0.40	0.10
	Modified Froude number	12.45	12.45
Kinematic Similarity	Operating temperature, K	1473	293
	Dynamic viscosity, Pas	0.01	0.0009
	Kinematic viscosity, m^2s^{-1}	0.000002	0.000001
	Liquid density, kgm^{-3}	4600	998
	Surface tension, Nm^{-1}	0.93	0.0728
	Slag density, kgm^{-3}	3300	774
	Slag/matte density ratio	0.717	0.775
	Morton number	$2.65x10^{-11}$	$2.65x10^{-11}$

2.2 Numerical simulation and model description

Experimental observation were numerically studied with CFD numerical code FLUENT version 12.1.4 on a 1.86GHz Intel(R) Core(TM)2 processor with 2GB RAM. Gambit 2.4.6 was used for geometry creation of the 2-D and 3-D domain as given in **Figure 2**.

Mesh quality affects the face flux calculations between cells and hence directly impacts the accuracy of the solution and ease of convergence. Computational cell skewness which is a measure of difference between the shape of the cell and the shape of an equilateral cell of equivalent area (for 2-D domain) or volume (for 3-D domain) was used as the mesh quality measurement criteria. Highly skewed computational cells can decrease accuracy and stability of the

solution. In both domains, over 97% of domain computation cells were falling in the high quality mesh with equisize skew values of less than 0.4. A size function and cooper tool method of meshing was used for the 3-D domain.

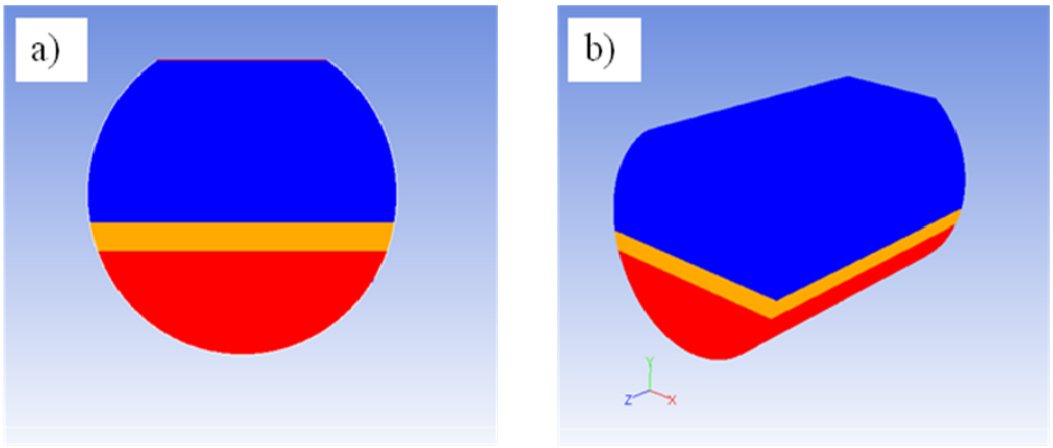

Figure 2: Computational geometry (a) 2-D and (b) 3-D domain as exported in FLUENT

Physical phenomena in closed systems for incompressible fluids are described fully by continuity (mass), momentum and energy conservation equations. These are incorporated in the volume of fluid (VOF) formulation describing the fluid dynamics.

2.3 Governing equations

The mass (continuity), momentum and energy conservation equations are given in **Eqs. (4)**, **(5)** and **(6)** respectively.

Mass (continuity) conservation equation

$$\frac{\partial}{\partial t}(\rho)+\nabla\cdot(\rho v)=S_m \tag{4}$$

Momentum conservation equation

$$\frac{\partial}{\partial t}(\rho u)+\nabla\cdot(\rho v u)=-\frac{\partial P}{\partial x}+\nabla\cdot(\mu\nabla u)+S_m \tag{5}$$

Energy conservation equation

$$\frac{\partial}{\partial t}(\rho E)+\nabla\cdot\left(\vec{v}(\rho E+P)\right)=\nabla\cdot\left(k_{eff}\nabla T-\sum_i h_i\vec{J}_i+\left(\bar{\bar{\tau}}_{eff}\cdot\vec{v}\right)\right)+S_E \tag{6}$$

DOI: 10.2202/1934-2659.1584

In this equation, k_{eff} is the effective thermal conductivity given by: $k_{eff} = k_T + k_t$, where k_t ($WK^{-1}m^{-1}$) is the turbulent thermal conductivity, defined according to the turbulence model being used, k_T ($WK^{-1}m^{-1}$) is thermal conductivity and $\bar{\bar{\tau}}_{eff}$ (Pa) is the effective stress tensor. The first three terms on the right-hand side of **Eq. (6)** represent energy transfer due to conduction, species diffusion and viscous dissipation respectively. S_E is the energy source term which includes the heat of chemical reaction, and any other volumetric heat sources defined in the model.

Depending on the nature of the problem, equations to be solved can be increased. In this work, conservation equation for chemical species was solved, predicting the local mass fraction of species, Y_i through the solution of a convection-diffusion equation for the ith species. The equation solved was as given below:

$$\frac{\partial}{\partial t}(\rho Y_i) + \nabla \cdot (\rho \vec{v} Y_i) = -\nabla \vec{J}_i + R_i + S_i \qquad (7)$$

In this equation, $\vec{J}_i$ is the diffusion flux of species i, which arises due to gradients of temperature and concentration, R_i is the net rate of production of species i by chemical reaction and S_i is the rate of creation by addition from the dispersed phase plus any user-defined sources. Since these above discussed mathematical statements (**Eqs. (4)**, **(5)**, **(6)** and **(7)**) are partial differential equations, they have to be discretized to algebraic equations and iterative method of solution implemented (ANSYS 2008). The subsequent sections fully describe the numerical models employed in this work to account for interphase tracking and turbulence.

2.4 Models

The VOF Model

The VOF model was chosen to account for the multiphase flow. Phase surface behaviour of water, kerosene and air was captured by this model using the Geo-Reconstruction scheme. This is accomplished through surface tracking of the phase interfaces by the solution of a VOF continuity equation (**Eq. (8)**) for the volume fraction of at least one of the phases in the system. In the model, the different phases are treated numerically as interpenetrating continua thus inevitably introducing the concept of phasic volume fraction where summation of

volume fraction in each computational cell sums to unity. In other words, if the *i*th fluid's volume fraction in the cell is denoted by α_i, then it follows that:

$\alpha_i = 0$: The computational cell is empty of the α_i fluid

$\alpha_i = 1$: The computational cell is full of the α_i fluid

$0 < \alpha_i < 1$: The computational cell contains at least one phase of α_i fluid

For the *i*th fluid phase, VOF equation has the following form:

$$\frac{\partial}{\partial t}(\alpha_i \rho_i) + \nabla \cdot (\alpha_i \rho_i v_i) = S_m \tag{8}$$

In the formulation, the volume fraction equation for the primary phase will not be solved but computed based on the constraint:

$$\sum_{i=1}^{n} \alpha_i = 1 \tag{9}$$

The k-ε turbulent model

In order to incorporate the effects of turbulence on the flow field inside the model, Realizable $k-\varepsilon$ model was implemented. This is a two equation model based on transport equations for the turbulence kinetic energy, k and its rate of dissipation, ε. It is a relatively recent development by Shih et al. (1995) which offers improvements in the overall energy transfer. The transport equation for k is derived from exact equation, while the transport equation for ε is obtained from physical reasoning. Turbulence variables k and ε are obtained from transport **Eqs. (10)** and **(11)** respectively.

$$\frac{\partial}{\partial t}(\rho k) + \frac{\partial}{\partial x_i}(\rho k u_i) = \frac{\partial}{\partial x_j}\left[\left(\mu + \frac{\mu_t}{\sigma_k}\right)\frac{\partial k}{\partial x_j}\right] + G_k + G_b - \rho\varepsilon - Y_M + S_k \tag{10}$$

DOI: 10.2202/1934-2659.1584

$$\frac{\partial}{\partial t}(\rho\varepsilon)+\frac{\partial}{\partial x_i}(\rho\varepsilon u_i)=\frac{\partial}{\partial x_j}\left[\left(\mu+\frac{\mu_t}{\sigma_\varepsilon}\right)\frac{\partial k}{\partial x_j}\right] + \rho C_1\varepsilon-\rho C_2\frac{\varepsilon^2}{k+\sqrt{v\varepsilon}}+C_{1\varepsilon}\frac{\varepsilon}{k}C_{3\varepsilon}G_b+S_\varepsilon \quad (11)$$

Generation of turbulence kinetic energy due to mean velocity gradients and turbulent viscosity is given by **Eqs. (12)** and **(13)** respectively

$$G_k=-\rho\overline{v_x^{'}v_y^{'}}\frac{\partial y}{\partial x} \quad (12)$$

$$\mu_t=\rho C_\mu\frac{k^2}{\varepsilon} \quad (13)$$

In equations above, $v_x^{'}$ and $v_y^{'}$ (ms^{-1}) are averaged fluid axial and radial velocity components respectively. Fundamentally, the effective viscosity in the momentum equations is the summation of molecular and turbulent viscosity given by:

$$\mu_{eff}=\mu+\mu_t \quad (14)$$

2.5 Phase physical properties

The properties appearing in the transport **Eq. (8)** are determined by the existence of the component phase in each computational cell. In a two phase system with phase volume fraction, α with subscripts *i* and *j*, summation of phase fraction in the computational cell subject to constraint imposed by **Eq. (9)** yields:

$$\alpha_i+\alpha_j=1 \quad (15)$$

The density of phase scripted by *i* in the computational cell will be given as:

$$\rho=\alpha_i\rho_i+(1-\alpha_i)\rho_j \quad (16)$$

All other physical properties like viscosity are computed in the same way.

2.6 Method of solution

The governing equations of flow, VOF equations, $k-\varepsilon$ turbulence model equations and species concentration equations (**Eqs. (4)**, **(5)**, **(6)**, **(7)**, **(8)**, **(10)** and **(11)**) were solved with CFD numerical code FLUENT version 12.1.4. This package is a finite volume solver using body-fitted computational grids. Semi empirical method for pressure linked equations (SIMPLE) algorithm was used for pressure-velocity coupling with geo-reconstruction scheme for obtaining face fluxes, when the computational cell is near the interface using piecewise-linear approach (ANSYS 2008). A time step of 0.001s was used and found to be sufficient for maintenance of numerical convergence at every time step and stability. Convergence of numerical solution was determined based on surface monitoring of integrated quantities of bulk flow velocity and turbulence and scaled residuals of continuity, x-, y-, z-velocities, k and ε. The residuals of all quantities were set to 10^{-3} and the solution was considered converged when all the residuals were less than or equal to the set value.

2.7 Mixing time measurements

A tracer dispersion technique using sulphuric acid and pH meter measurements was used in this work to measure the mixing time, T_{mix} (response) in the converter model. 6ml of 98% sulphuric acid (H_2SO_4) was used as the tracer in each experiment and injected in the centre of the model at 100mm below the water (simulated matte) level.

In this work, the midpoint of the bath was taken as the tracer injection point for simulation of converter inputs charging point which is situated in the centre of industrial Peirce – Smith converter. A pH meter was placed directly opposite the tracer injection point at 100mm from the converter circular wall. **Figure 3** shows tracer-pH meter positioning as used in this experimental set-up.

Water was filled to a total constant height of 270mm which is 39% filling capacity. Kerosene to water height ratio was varied from 0% to 40% at five equidistant intervals. Air volumetric flow rate, was varied from $0.00875 Nm^3s^{-1}$ to $0.01375 Nm^3s^{-1}$ which represents typical scaled down industrial operation range. A matrix of 25 experiments was done and each experimental condition was repeated 5 times. An average mixing time was taken which was within 10% standard deviation on all experimental conditions. The response T_{mix} was defined as the amount of time taken to achieve uniform and homogeneous steady state concentration of the bath after introducing a tracer which was measured as decay in pH concentration to a value +/-0.01pH units presenting 99% mixing.

DOI: 10.2202/1934-2659.1584

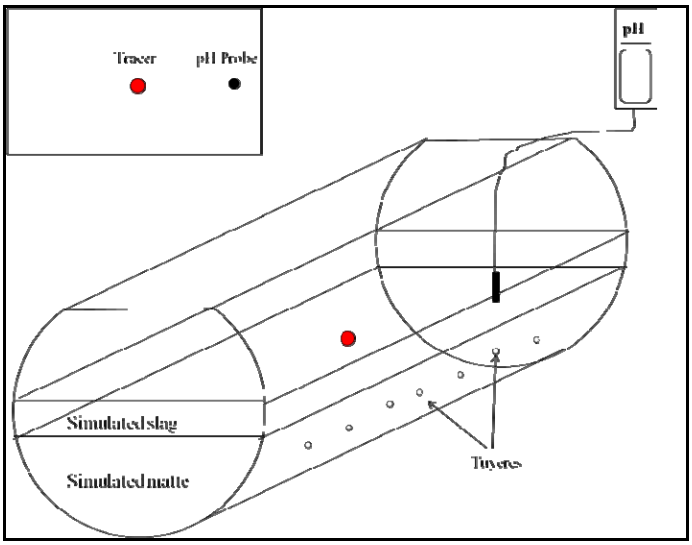

Figure 3: Schematic 3-D view of the model showing tracer and pH probe arrangement as used in the mixing experiments

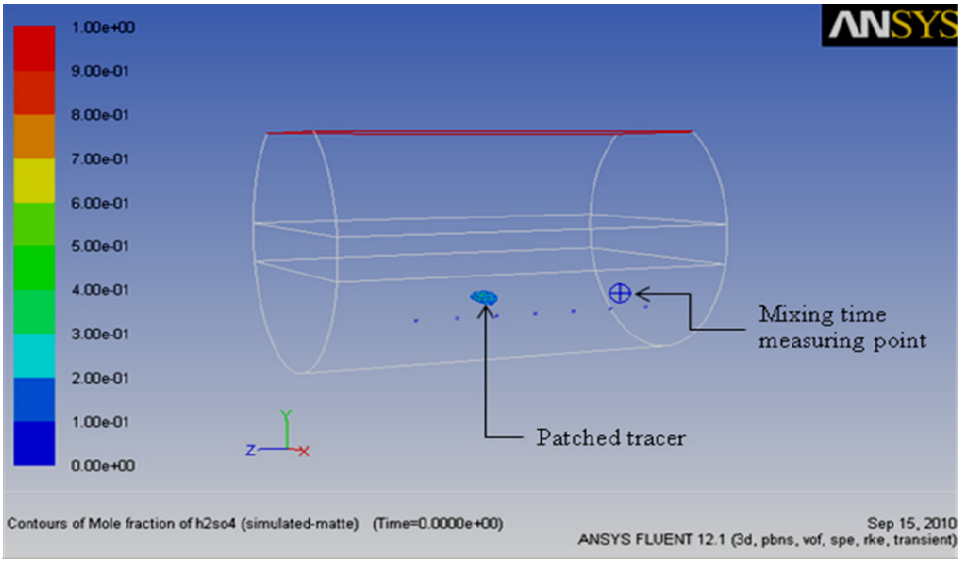

Figure 4: Tracer patching and custom field function (measuring point) position

In the numerical simulations for mixing time measurements, a region was adapted in the same location as the tracer injection point in the physical experiments where acid was patched as given in **Figure 4** with a volume fraction of 1. A custom field function was formulated at the position analogous to the pH

position, measuring the mole fraction of tracer species concentration as a function of flow time producing typical concentration time graph as given in **Figure 5**. This was achieved through solving the species transport equation given in **Eq. (7)**. Mixing was considered complete when the species concentration reaches a stable value on the apex of the curve.

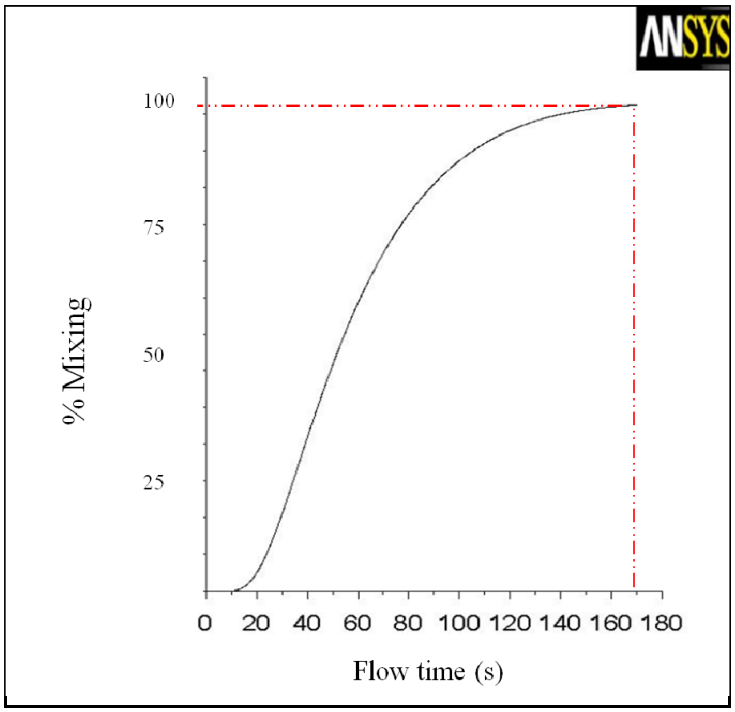

Figure 5: Generic numerical mixing time measurement curve

3. RESULTS AND DISCUSSION

In interpretation of the results of the effects of flow rate on physical mixing simulations, the volumetric air flow rates were converted to specific mixing power, ε_m which is defined as the rate of work done per unit mass of the liquid phase by the purged air. Through integration of summation of work done by buoyancy and work done by rising bubble in gas systems assuming ideal gas behaviour in limits of injection submergence, H_s (m), buoyancy specific power, ε_b (kWton^{-1}) is given in **Eq. (17)**(Brimacombe et al. 1985).

$$\varepsilon_b = \frac{2QP_a}{W}\ln\left(1+\frac{\rho g H_s}{P_a}\right) \tag{17}$$

DOI: 10.2202/1934-2659.1584

However, Nilmani & Das (1995) and Turkoglu & Farouk (1991) alluded that the specific power due to gas kinetic energy, ε_k at small vessel aspect ratio is quite significant. Specific power due to gas kinetic energy ε_k is given by:

$$\varepsilon_k = \frac{\rho_g Q^3}{2WA^2} \tag{18}$$

Where W (kg) is effective bath weight, Q (Nm^3s^{-1}) is total gas flow rate, P_a (kPa) is atmospheric pressure and A (m^2) is total tuyere cross sectional area.

Thus, the specific mixing power, ε_m to the system was calculated as an algebraic summation of buoyancy and kinetic specific power given by:

$$\varepsilon_m = \varepsilon_b + \varepsilon_k \tag{19}$$

In this study, measured mixing time against specific mixing power at different air volumetric flow rates are shown in **Figure 6**. Simulated slag presence has been observed to present a complex phase interaction phenomena.

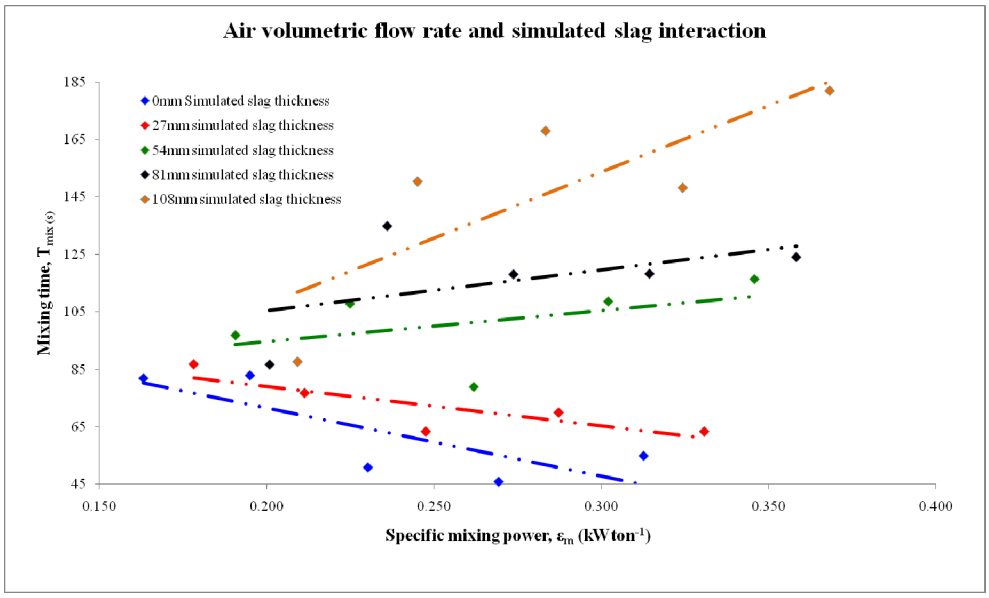

Figure 6: Effect of air volumetric flow rate on mixing time

In **Figure 6**, there appears to be two different bands of mixing time distributions, one with no and/ or with thin simulated slag layer and the other one is with high simulated slag thickness. Mixing time was observed to decrease with

increase in specific mixing power for the cases with no and with thin simulated slag thickness. The figure shows that, beyond a critical simulated slag depth, the mixing time will increase with an increase in specific power of mixing. With high simulated slag thickness of 54mm and above, this trend shifted to an increased mixing time with increase in specific mixing power.

The observed increase in mixing times with increased specific mixing power is in consistent with the results obtained by Valencia et al. (2004). In their studies, they observed that increase in air power is used to generate more turbulence conditions in the converter, with little benefits in terms of mixing quality in the mean flow of the bath. In our study, **Figure 7** shows turbulence kinetic energy vector plots for 54mm and 108mm simulated slag thickness.

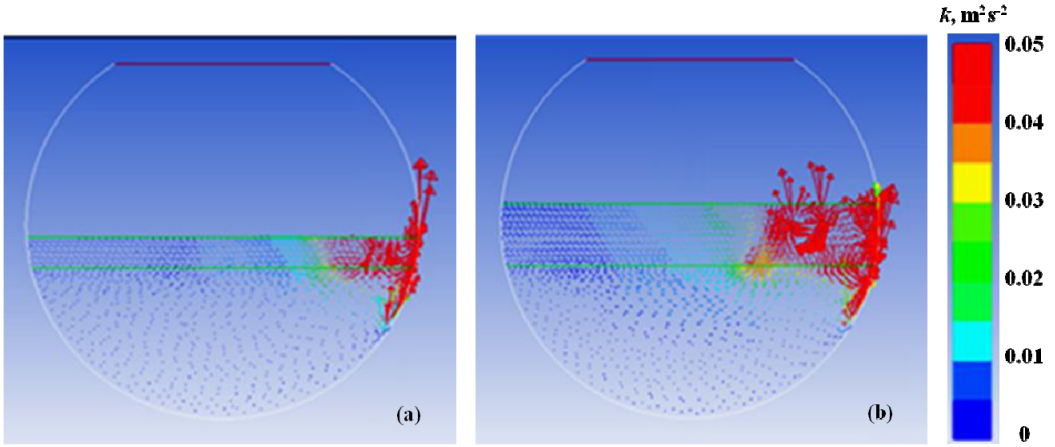

Figure 7: Turbulence kinetic energy vector plots for (a) 54mm and (b) 108mm simulated slag thickness at air flow rate of 0.01125Nm^3s^{-1}

It is quite evident from **Figure 7** that high turbulent conditions are created and concentrated in the tuyere region that subsequently results in substantial slopping and splashing. With increase in air power, potential energy for recirculation and mixing is wasted to the converter free space.

3.1 Mixing Time Correlation

In this work, it was assumed that all the specific power due to buoyancy and gas kinetic energy supplied contributed towards model agitation. As observed from **Figure 6**, the two different bands of mixing distributions are presented by two separate regression analysis equations. Mixing time results for 27mm and 108mm simulated slag thickness were analysed representing low slag and high slag

DOI: 10.2202/1934-2659.1584

operations respectively. Two separate mixing times $T_{mix,low-slag}$ and $T_{mix,high-slag}$ in terms of total specific mixing power, ε_m as given in **Figure 8** was suggested.

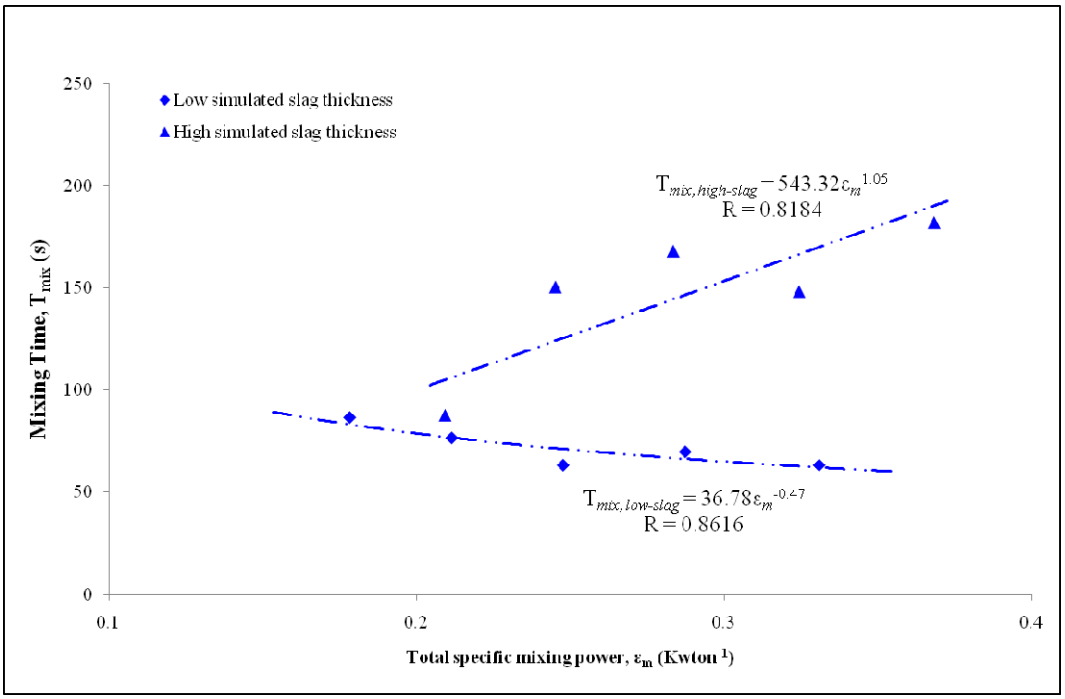

Figure 8: Correlation between mixing time and specific mixing power

The above analysis provided the relationship: $T_{mix,low-slag} = 36.78\varepsilon_m^{-0.47}$ and $T_{mix,high-slag} = 543.32\varepsilon_m^{1.05}$ for estimating mixing time in the PSC model for low simulated slag and high simulated slag thicknesses respectively.

$$T_{mix,low-slag} = 36.78\varepsilon_m^{-0.47} \quad (20)$$

$$T_{mix,high-slag} = 543.32\varepsilon_m^{1.05} \quad (21)$$

The average value for the ratio of specific power due to gas kinetic energy to specific power due to buoyancy $\left(\frac{\varepsilon_k}{\varepsilon_b}\right)$ was calculated to be:

$$\frac{\varepsilon_k}{\varepsilon_b} = 0.21 \quad (22)$$

Hence it follows from **Eq. (19)** that,

$$\varepsilon_m = 5.76\varepsilon_k \tag{23}$$

Since $\varepsilon_k = \dfrac{\rho_g Q^3}{2WA^2}$ from **Eq. (18)**, the mixing time correlation **Eq. (20)** and **Eq. (21)** may be expressed as:

$$T_{mix,low-slag} = 36.78\left(5.76\frac{\rho_g Q^3}{2WA^2}\right)^{-0.47} \tag{24}$$

$$T_{mix,high-slag} = 543.32\left(5.76\frac{\rho_g Q^3}{2WA^2}\right)^{1.05} \tag{25}$$

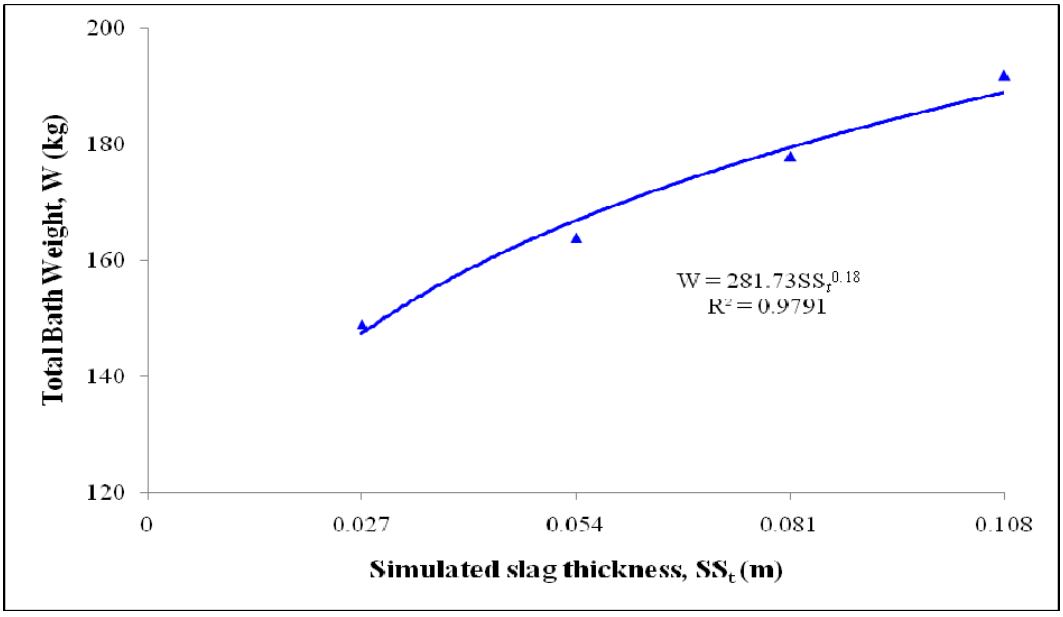

Figure 9: Relationship between total bath weight and simulated slag thickness

In the current study, bath weight, W in kg was a summation of simulated matte and simulated slag with simulated matte weight kept constant at 135kg in the model. Regression analysis of the simulated slag thickness, SS_t and the total

DOI: 10.2202/1934-2659.1584

bath weight, W associated with the quantity of simulated slag yielded results shown in **Figure 9**.

$$W = 281.73 SS_t^{0.18} \tag{26}$$

Substituting **Eq. (26)** into **Eqs. (24)** and **(25)** yields application oriented correlations for mixing time estimation in the PSC model respectively as:

$$T_{mix,low-slag} = 0.164 Q^{-1.41} SS_t^{0.08} \tag{27}$$

And,

$$T_{mix,high-slag} = 96767403 Q^{3.15} SS_t^{-0.19} \tag{28}$$

It is presumed that at thin simulated slag thickness, the effect of interphase interaction i.e. interphase friction, interphase diffusion, and two-phase turbulence modification in bath recirculation, is not yet fully developed hence the reduced mixing times observed.

Numerical simulations have revealed that in thin simulated slag thicknesses, all slag is pushed to tuyere line opposite side with the plume region being composed of almost only matte as shown in **Figure 10**. This increases hydrodynamic pressure to the rising bubbles and hence increased specific energy dissipated to the liquid phase for bath recirculation due to high bubble retention time thus increased mixing efficiency.

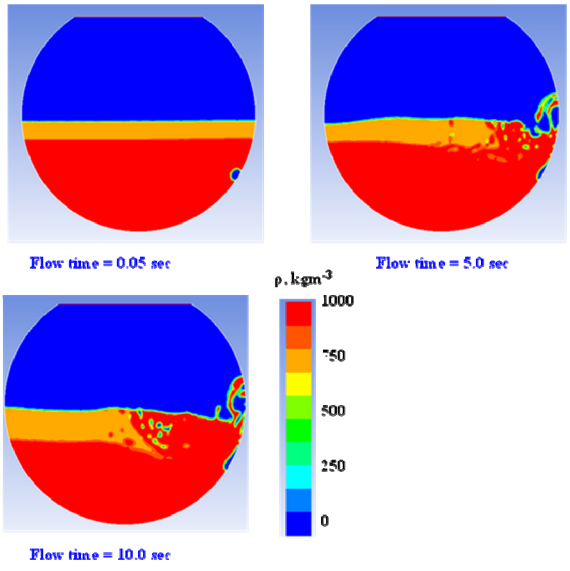

Figure 10: 2-D density contour plots with 54 simulated slag thickness at 0.01125Nm^3s^{-1}

However, the benefits of such retention time are offset by the effects of phase interaction, friction and diffusion mechanism which dissipates substantial amount of energy at high slag volumes. Mechanisms of momentum transfer at simulated matte-simulated slag-air interfaces fritter away potential recirculation energy. At increased simulated slag thickness of 108mm, as can be seen in **Figure 11**, numerical simulation, the effect of interaction and dispersion is highly pronounced. As such, mixing in the simulated matte phase is expected to decrease. There is also reduced effective interphase exchange momentum due to dissipation of energy by the simulated slag as a result of localized secondary recirculation flows which is more pronounced at high simulated slag volumes.

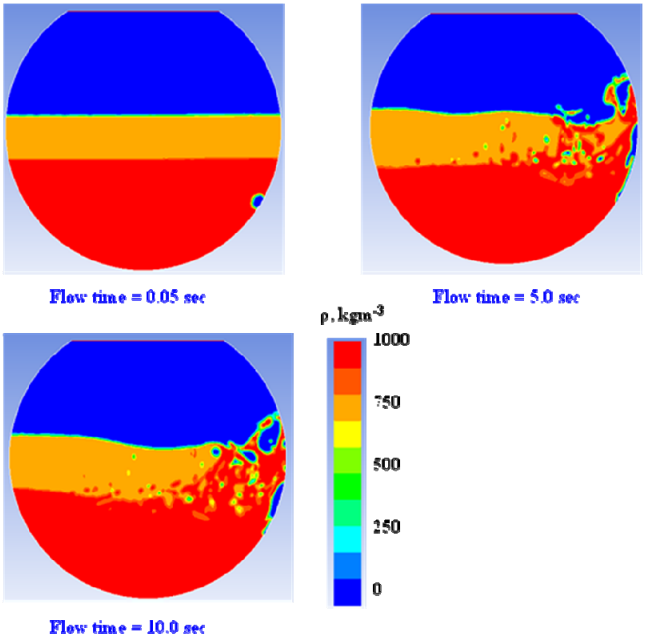

Figure 11: 2-D density contour plots with 108 simulated slag thickness at 0.01125Nm^3s^{-1}

This observation is in agreement with the results obtained by Han et al. (2001) in their investigation of flow characteristics in a gas stirred ladle using oil and water in their model vessel.

As pointed out by Turkoglu & Farouk (1991), liquid bulk circulation rate is inversely proportional to mixing time which indicates that the bulk motion of the liquid plays an important role in mixing which also suggests that liquid recirculation rate can be used as a measure of mixing efficiency.

DOI: 10.2202/1934-2659.1584

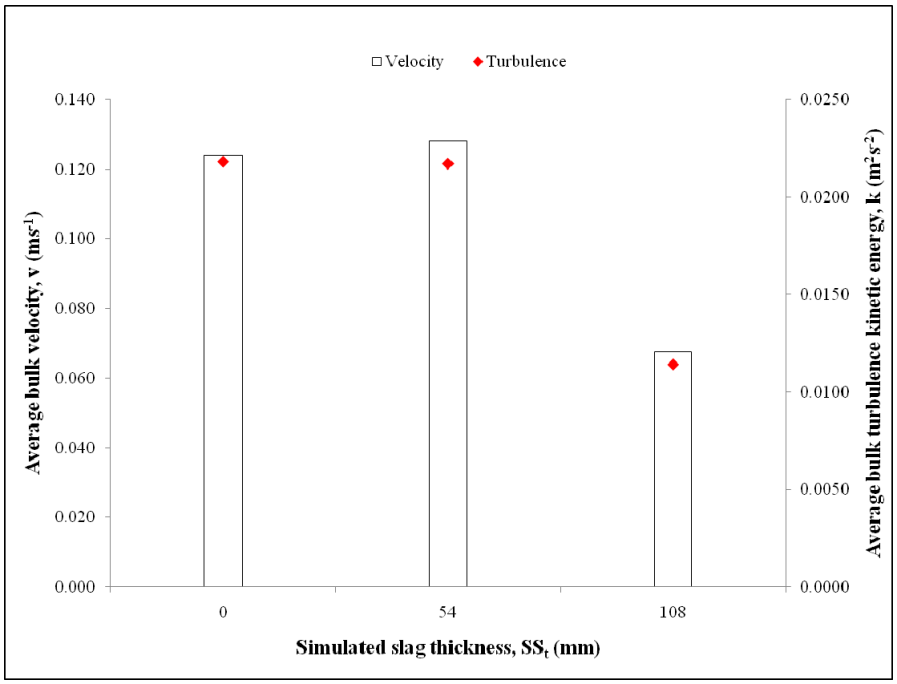

Figure 12: Variation of average simulated matte bulk flow velocity and turbulence kinetic energy as a function of simulated slag thickness at $0.01125 Nm^3s^{-1}$

Figure 12, as extracted from numerical simulation results in this study, shows the variation of average bulk velocity and turbulence kinetic energy with simulated slag height. Average bulk velocity was calculated as the average of velocity in infinite sampling points in the simulated matte calculation domain. It could be seen from this figure that at 54mm simulated slag thickness and above, the bulk recirculation velocity is reduced thereby increasing the mixing time.

There appears to be two different bands of average bulk velocity and turbulence set up in the converter, which occurs at low air flow rates and high flow rates derived from this work. At low air flow rate, average bulk velocity decreases proportionally with increase in simulated slag thickness which is attributable to increased process quantities against constant process driving power which is air input. It could be reasoned that phase interactions are not fully developed with such flow rate such that the two phases acts as one continuous phase with mild and negligible interactions. At high flow rates, this behaviour is altered due to enhanced process driving power which causes strong and intense interaction of phases.

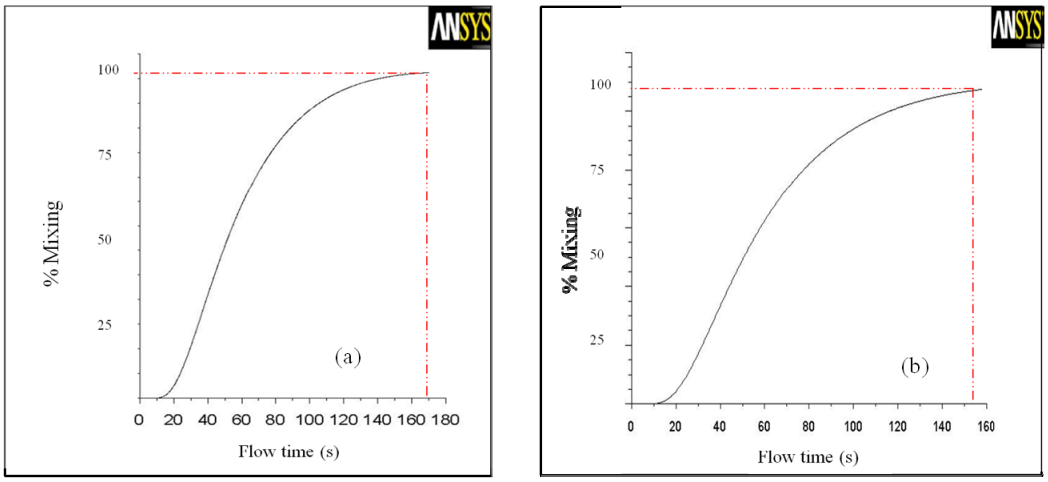

Figure 13: Numerical mixing time results for (a) 270mm matte and 108mm simulated slag thickness case and (b) equivalent total simulated matte depth of 378mm at air volumetric flow rate of 0.01125Nm^3s^{-1}

In an effort to understand if increased mixing times in the multiphase system was due to phase interactions, mixing time numerical simulations were also done with equivalent heights of only matte and matte plus simulated slag of which simulated slag was 108mm. Numerical simulations with only simulated matte depth show improved mixing efficiency as shown in **Figure 13**, were mixing time decreased from 168 sec to 153 sec. This could be attributed to improved gas bubble – bulk liquid momentum transfer due to high gas retention time as well as absence of energy dissipation in recirculation flow hence increased mixing efficiencies.

Therefore, the observed decrease in mixing efficiency at higher simulated slag thickness could be attributed to three-fold effect namely; channelling, manifestation of phase interaction between simulated matte and simulated slag and tuyere flow dynamics.

However, if one extrapolates these findings to the current typical PSC, the tuyere submergence is relatively shallow and as such, increase in air volumetric flow rate will result in a channelling effect where the bulk of the mixing efficiency is directed to the bath surface thereby reducing the amount of momentum transfer to the bulk of the liquid. This situation can be aggravated by the presence of slag which will dissipate some of the energy.

Bulk turbulence kinetic energy generated in the bath is affected in the same way as the bulk velocity as shown in **Figure 12**. Turbulence kinetic energy was calculated as the average of turbulence kinetic energy in infinite sampling points in the simulated matte calculation domain. Generally turbulence was observed to decrease with increasing simulated slag height which translated to increased mixing time.

DOI: 10.2202/1934-2659.1584

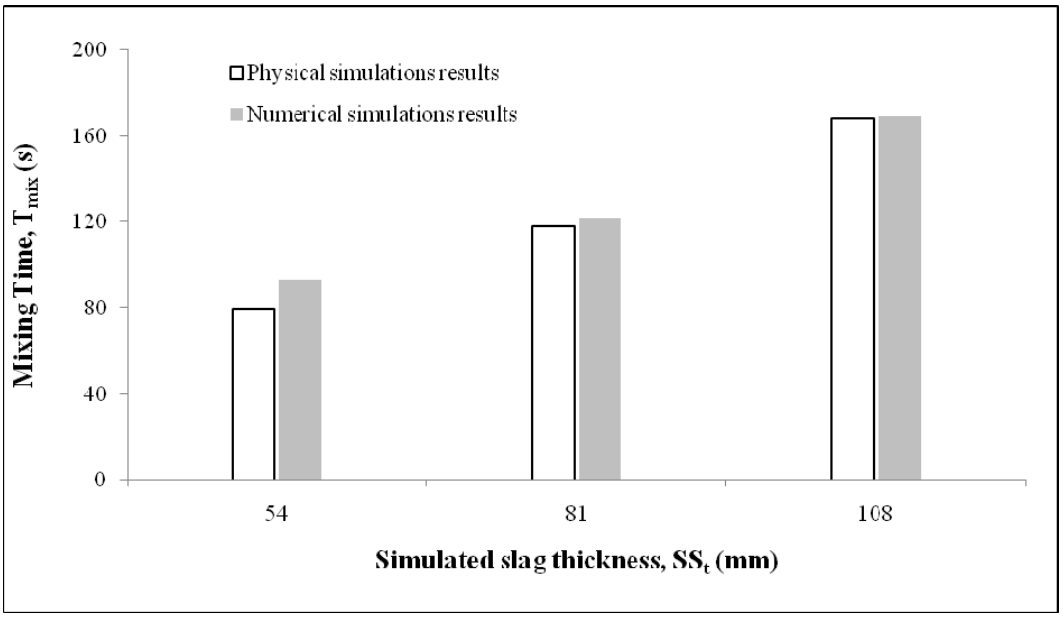

Figure 14: Comparison of numerical and physical mixing time measurements at air flow rate of 0.01125Nm^3s^{-1}

Numerical and physical simulation results for mixing are depicted in **Figure 14**. As can be seen, both numerical and physical simulation shows a great deal of agreement between them. Numerical simulation results in **Figures 15** give the bulk velocity distributions and turbulence in the converter in the tuyere line plane.

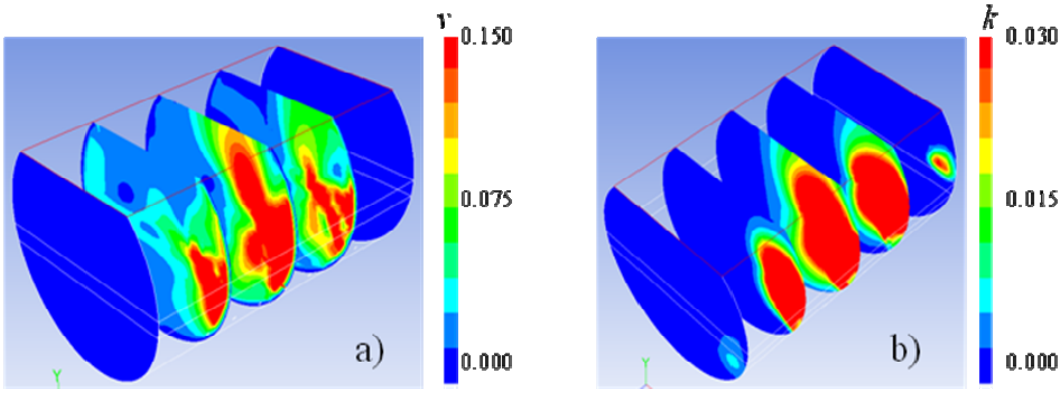

Figure 15: Contours of simulated a) bulk velocity b) turbulence kinetic energy after 5sec of simulation (Blow rate = 0.01125Nm^3s^{-1}, simulated slag thickness =108mm)

The distribution of flow field variables in terms of velocity and turbulence is more skewed and concentrated on the tuyere line of the converter. These observations have confirmed that there might be a unique liquid transport mechanism taking place in the converter. This is because, although bulk velocity profiles are skewed in such a way that one would expect the presence of extensive dead zones in the model converter, it is seemingly becoming homogeneously mixed in short periods of times. Therefore, eddy diffusion and bulk convection could be postulated to be the driving liquid flow mechanism. Regions containing air are included in the contour plots.

3.2 Process Implications of Results

When the liquid height in the PSC is generally low, the gas channels though the liquid along the vertical side wall of tuyere injection nozzle axis. In that case residence time of the gas bubbles inside the melt is reduced; this in turn reduces gas-liquid interactions within the bulk liquid. Therefore, as a result of channelling, the effectiveness of the gas momentum and power transfer to the bulk liquid flow is reduced. This adversely affects the mixing, liquid-liquid and liquid-solid mass transfer activities within the bath. On the other hand, with an increase in liquid height in the converter, the axial gas-liquid plume residence time increases and hence there is more interaction between the gas and liquid. This will lead to more matte entrainment into the rising plume and a stronger agitation in the bath. In order to maintain consistent mixing power and counteract the adverse circumstances presented by the rising liquids volumes, the bath height with respect to matte and slag ratio should be monitored in order to make necessary adjustments to the gas blowing rates for a more energy efficient process.

4. CONCLUSSIONS

In this study, the influence of simulated slag layer on mixing characteristics and behaviour in an industrial Peirce-Smith converter (PSC) has been studied experimentally using cold model simulation. The 2-D and 3-D simulations of the three phase system were also carried out using volume of fluid (VOF) and realizable $k-\varepsilon$ turbulence model to account for the multiphase and turbulence nature of the flow respectively. Numerical simulation results were found to be in good agreement with experimental results. On the basis of the above results and discussions, the main findings of this study are as follows:

- There exists a critical simulated slag thickness in the Peirce-Smith converter model, above which, increasing air flow rate results in extended mixing times due to a combination of channelling and secondary ecirculation in the simulated slag.

DOI: 10.2202/1934-2659.1584

- Secondary recirculation results in dissipation of energy resulting in reduced bulk fluid flow recirculation velocity and turbulence kinetic energy.
- Increased matte fraction in slag and matte systems increases mixing efficiencies possibly due to high bubble retention.
- High slag volumes are detrimental to the process efficiency as they results in dissipation of potential energy in the converter.
- It was revealed that the simulated slag layer as well as air flow rates has a great influence on the bulk recirculation velocity, turbulence and thus affecting mixing efficiency in the Peirce-Smith converter. This led to the proposed mixing times correlations based on air flow rate and slag layer thickness.

GLOSSARY

2-D		2-Dimensional
3-D		3-Dimensional
CFD	-	Computational Fluid Dynamics
Gambit	-	Geometry and Mesh Building Intelligent Toolkit
PSC	-	Peirce-Smith converter
RKE	-	Realizable $k-\varepsilon$ model
VOF	-	Volume of Fluid
VF	-	Volume Fraction

NOMENCLATURE

A	Total cross sectional/ interfacial area	m^2
C_D	Drag coefficient	
d_o	Tuyere diameter	mm
$D_{i,m}$	Mass diffusion coefficient for i th species in the mixture	

$D_{T,i}$	Thermal diffusion coefficient for i th species in the mixture	
D_t	Turbulent diffusivity	m^2s^{-1}
E	Total energy	J
F_D	Drag force	N
g	Gravitational constant	ms^{-2}
G_k	Turbulent kinetic energy generation due to mean velocity gradients	m^2s^{-2}
G_b	Turbulent kinetic energy generation due to buoyancy	m^2s^{-2}
i , j	Species	
I	Turbulent intensity	
$\vec{J}$	Diffusion flux	$molm^{-2}s^{-1}$
$\vec{J}_i$	Diffusion flux of i th species	$molm^{-2}s^{-1}$
k_{eff}	Effective thermal conductivity	$WK^{-1}m^{-1}$
k_t	Turbulent thermal conductivity	$WK^{-1}m^{-1}$
k_T	Thermal conductivity	$WK^{-1}m^{-1}$
k	Turbulent kinetic energy	m^2s^{-2}
l_{model}	Model physical dimension	m
l_{ptype}	Prototype (real) converter physical dimension	m
N^*_{Fr}	Modified Froude number	
N_{Mo}	Morton number	
P	Static pressure	Pa

DOI: 10.2202/1934-2659.1584

Q	Air volumetric flow rate	Nm^3s^{-1}
R_i	Net rate production of i th species by chemical reaction	
S_m , S_ε	Mass and turbulent dissipation source terms	
S_E , S_k	Energy and turbulent kinetic energy source terms	
T_{mix}	Mixing time	s
v_t	Tuyere gas velocity	ms^{-1}
v_x , v_y , v_z	x, y, z- velocity components	ms^{-1}
v_p	Particle velocity	ms^{-1}
$\vec{v}$	Overall velocity vector	ms^{-1}
Y_i	Local mass fraction of i th species	
Y_M	Contribution of the fluctuating dilatation in turbulence	

SYMBOLS

ϕ	Scalar quantity (Temperature, Turbulence, e.t.c)	
α	Fluid phase fraction	
μ	Dynamic viscosity	Pas
σ	Surface tension	Nm^{-1}
ρ_g , ρ_l	Density of gas and liquid respectively	kgm^{-3}
λ	Scale factor	

REFERENCES

ANSYS, I., 2008. User's Guide. *Fluent 6.3,*

BRIMACOMBE, J.K., BUSTOS, A.A., JORGENSEN, D. and RICHARDS,G.G., 1985. Towards a basic understanding of injection, *Physical chemistry of extractive metallurgy: proceedings of an international symposium* 1985, TMS, pp. 327.

CASTILLEJOS, A.H. and BRIMACOMBE, J.K., 1987. Measurement of physical characteristics of bubbles in gas-liquid plumes: Part II. Local properties of turbulent air-water plumes in vertically injected jets. *Metallurgical and Materials Transactions B,* **18**(4), pp. 659-671.

GONZALEZ, J., REAL, C., PALOMAR-PARDAVE, M., HOYOS, L., GUTIERREZ, M. and MIRANDA, R., 2008. CFD simulation gas-liquid flow in a copper converter with bottom air injection. *International Journal of Chemical Reactor Engineering,* **6**(6), pp. 54.

GRAY, N.B., NILMANI, M. and FOUNTAIN, C.R., 1984. Investigation and modelling of gas injection and mixing in molten liquid processes. *The Aus.I.M.M Melbourne branch, Symposium on Extractive Metallurgy,* , pp. 269-277.

HAN, J.W., HEO, S.H., KAM, D.H., YOU, B.D., PAK, J.J. and SONG, H.S., 2001. Transient fluid flow phenomena in a gas stirred liquid bath with top oil layer—Approach by numerical simulation and water model Experiments. *ISIJ International,* **41**(10), pp. 1165-1172.

HOEFELE, E.O. and BRIMACOMBE, J.K., 1979. Flow regimes in submerged gas injection. *Metallurgical and Materials Transactions B,* **10**(4), pp. 631-648.

KIM, S.H. and FRUEHAN, R.J., 1987. Physical modeling of liquid/liquid mass transfer in gas stirred ladles. *Metallurgical and Materials Transactions B,* **18**(2), pp. 381-390.

KOOHI, A.H.L., HALALI, M., ASKARI, M. and MANZARI, M.T., 2008. Investigation and Modeling of Splashing in the Peirce Smith Converter. *Chemical Product and Process Modeling,* **3**(1), pp. 2.

KYLLO, A.K. and RICHARDS, G.G., 1998a. A kinetic model of Pierce Smith Converter: Part I. Model formulation and validation. *Metallurgical Transactions B,* **29B**, pp. 239-250.

KYLLO, A.K. and RICHARDS, G.G., 1998b. A kinetic model of Pierce Smith Converter: Part II. Model application and discussion. *Metallurgical Transactions B,* **29B**, pp. 251-259.

LIOW, J.L. and GRAY, N.B., 1990. Slopping resulting from gas injection in a Pierce-Smith Converter: Water model. *Metallurgical and Materials Transactions B,* **21**(6), pp. 987-996.

DOI: 10.2202/1934-2659.1584

MAZUMDAR, D., 1990. Dynamic similarity considerations in gas-stirred ladle systems. *Metallurgical and Materials Transactions B,* **21**(5), pp. 925-928.

MAZUMDAR, D. and GUTHRIE, R.I.L., 1986. Mixing models for gas stirred metallurgical reactors. *Metallurgical and Materials Transactions B,* **17**(4), pp. 725-733.

NILMANI, M. and DAS, A.K., 1995. Bubble overlap in multipoint gas-injection systems. *Metallurgical and Materials Transactions B,* **26**(1), pp. 1147-1156.

NYOKA, M., AKDOGAN, G., ERIC, R.H. and SUTCLIFFE, N., 2003. Mixing and solid-liquid mass transfer rates in a Creusot Loire Uddeholm vessel: A water model case study. *Metallurgical and Materials Transactions B,* **34**(6), pp. 833-842.

RAMIREZ-ARGAEZ, M.A., 2008. Numerical simulation of fluid flow and mixing in gas-stirred ladles. *Materials and Manufacturing Processes,* **23**(1), pp. 59-68.

REAL, C., HOYOS, L., CERVANTES, F., MIRANDA, R., PALOMAR-PARDAVE, M., BARRON, M. and GONZALEZ, J., 2007. Fluid characterization of copper converters. *Mecánica Computacional,* **26**, pp. 1311-1323.

ROSALES, M., FUENTES, R., RUZ, P. and GODOY, J., 1999. A fluid dynamic simulation of a Teniente Converter. *Copper 99- Cobre 99,* , pp. 107-121.

ROSALES, M., VALENCIA, A. and FUENTES, R., 2009. A Methodology for Controlling Slopping in Copper Converters by Using Lateral and Bottom Gas Injection. *International Journal of Chemical Reactor Engineering,* **7**(1), pp. 1868.

SAHAI, Y. and GUTHRIE, R.I.L., 1982. Hydrodynamics of gas stirred melts: Part I. Gas/liquid coupling. *Metallurgical and Materials Transactions B,* **13**(2), pp. 193-202.

SCHWARZ, M.P., 1996. Simulation of gas injection into liquid melts. *Applied Mathematical Modelling,* **20**(1), pp. 41-51.

SHIH, T.H., LIOU, W.W., SHABBIR, A., YANG, Z. and ZHU, J., 1995. A new k-[epsilon] eddy viscosity model for high Reynolds number turbulent flows. *Computers & Fluids,* **24**(3), pp. 227-238.

SINHA, U.P. and MCNALLAN, M.J., 1985. Mixing in ladles by vertical injection of gas and gas-particle jets—A water model study. *Metallurgical and Materials Transactions B,* **16**(4), pp. 850-853.

STAPUREWICZ, T. and THEMELIS, N.J., 1987. Mixing and Mass Transfer Phenomena in Bottom-Injected Gas--Liquid Reactors. *Can.Metall.Q.,* **26**(2), pp. 123-128.

TURKOGLU, H. and FAROUK, B., 1991. Mixing time and liquid circulation rate in steelmaking ladles with vertical gas injection. *ISIJ International,* **31**(12), pp. 1371-1380.

VAARNO, J., PITKÄLÄ, J., AHOKAINEN, T. and JOKILAAKSO, A., 1998. Modelling gas injection of a Peirce-Smith-converter. *Applied Mathematical Modelling,* **22**(11), pp. 907-920.

VALENCIA, A., CORDOVA, M. and ORTEGA, J., 2002. Numerical simulation of gas bubbles formation at a submerged orifice in a liquid. *International Communications in Heat and Mass Transfer,* **29**(6), pp. 821-830.

VALENCIA, A., PAREDES, R., ROSALES, M., GODOY, E. and ORTEGA, J., 2004. Fluid dynamics of submerged gas injection into liquid in a model of copper converter. *International Communications in Heat and Mass Transfer,* **31**(1), pp. 21-30.

VALENCIA, A., ROSALES, M., PAREDES, R., LEON, C. and MOYANO, A., 2006. Numerical and experimental investigation of the fluid dynamics in a Teniente type copper converter. *International Communications in Heat and Mass Transfer,* **33**(3), pp. 302-310.

ZHU, M.Y., SAWADA, I., YAMASAKI, N. and HSIAO, T.C., 1996. Numerical simulation of three-dimensional fluid flow and mixing process in gas-stirred ladles. *ISIJ International,* **36**(5), pp. 503-511.

DOI: 10.2202/1934-2659.1584